Intermetallics 28 (2012) 58–64

Contents lists available at SciVerse ScienceDirect

Intermetallics

journal homepage: www.elsevier.com/locate/intermet

Instrumented indentation of transforming and no-transforming phases in Cu–Al–Be shape-memory alloys

S. Montecinos [a,b,*], A. Cuniberti [a,b], S. Simison [b,c]

[a] Instituto de Física de Materiales Tandil-IFIMAT, Facultad de Ciencias Exactas, Universidad Nacional del Centro de la Provincia de Buenos Aires, Pinto 399, 7000 Tandil, Argentina
[b] CONICET, Argentina
[c] INTEMA, Facultad de Ingeniería, Universidad Nacional de Mar del Plata, Juan B. Justo 4302, 7600 Mar del Plata, Argentina

ARTICLE INFO

Article history:
Received 27 December 2011
Received in revised form
16 March 2012
Accepted 29 March 2012
Available online 19 May 2012

Keywords:
B. Shape-memory effects
B. Martensitic transformations
B. Precipitates
F. Mechanical testing
B. Elastic properties

ABSTRACT

The behavior of Cu–Al–Be alloys under instrumented indentation using a Berkovich tip was studied. The pseudoelastic effect was evidenced in the transforming β Cu–Al–Be phase as a closed hysteresis loop between the unloading–reloading paths in the *P–h* curves and high depth recovery ratios. From series of indentations conducted in the $(\beta + \gamma_2)$ specimens, it was found that the indentation response of the two phases is remarkably different. Unlike the pseudoelastic β phase, γ_2 precipitates present an elastic–plastic behavior, obtaining a complete coincidence between the unload and reload path in the load–displacement curves, and a lower recovery capacity. An average contact pressure *versus* the penetration depth curve was estimated for each indentation curve, and results suggest that 8 GPa and 3 GPa can be considered an elastic limit for γ_2 and β phase respectively under Berkovich indenter stress state. The elastic modulus and the hardness of both phases were estimated from load–displacement curves using the Oliver and Pharr method.

1. Introduction

Shape-memory alloys can exhibit, within a certain range of temperatures, the pseudoelastic effect associated with the martensitic transformation of β phase. In the Cu–Al–Be system, β phase is stable at high temperatures, although it can be retained at temperatures below the stability region by rapid cooling. The β phase is bcc with long range order DO_3, and undergoes to a martensitic transformation by cooling, spontaneous transformation, or under mechanical stress. The martensitic phase is 18R, and it can be derived from an fct structure by introducing stacking faults on each third plane. The critical transformation temperature as well as the critical transformation stress is strongly dependent on the chemical composition. The pseudoelastic effect (PE) takes place when the martensitic transformation is stress-induced under appropriated conditions. The stress–strain loading curve shows a first linear part corresponding to the elastic regime of the β phase, a linearity deviation indicates the β to martensite transformation start, and a new almost linear stage corresponds to the progression of the martensitic transformation. On removing the load, a hysteretic loop is formed, and the strain is almost fully recovered leading to the PE behavior. Several studies about the thermomechanical and pseudoelastic behavior induced by tensile and compressive test of Cu–Al–Be alloys have been reported [1–7]. These alloys present large reversible strains, around 8% by compressive tests, and high damping capacities with values near to those reported for Ni–Ti alloys under similar conditions [5,8]. The instrumented indentation technique is being increasingly used to study the behavior of SMA at very small length scales, particularly in NiTi SMA [9–13], and fewer in Cu–Al–Ni [14,15]. However, the analysis of the load–displacement curves obtained by instrumented indentation presents a greater difficulty respect to those obtained by tensile and compressive tests due to the complex loading conditions. Evidence of the martensitic phase transformation induced by indentation has been previously reported as hysteresis loops produced between the unloading and reloading load–displacement curve [9,12]. In contrast, elastic–plastic materials present coincident unloading–reloading paths [16].

In this work, we present experiments of instrumented indentation on two phases in the same Cu–Al–Be alloys, the β phase,

* Corresponding author. Instituto de Física de Materiales Tandil-IFIMAT, Facultad de Ciencias Exactas, Universidad Nacional del Centro de la Provincia de Buenos Aires, Pinto 399, 7000 Tandil, Argentina. Tel.: +54 (0) 249 4439670; fax: +54 (0) 249 4439679.
E-mail address: dmonteci@exa.unicen.edu.ar (S. Montecinos).

0966-9795/$ – see front matter © 2012 Elsevier Ltd. All rights reserved.
doi:10.1016/j.intermet.2012.03.057

which transforms martensitically, and the γ_2 phase, which is a non-transforming phase. γ_2 phase was induced by precipitation under thermal treatments. It is the high aluminum stable phase, a complex cubic structure with stoichiometry Cu_9Al_4, coherent with the β matrix [17–20]. Because of the micrometer size of precipitates, microindentation becomes a powerful technique for its study.

2. Experimental procedure

Cu-22.66Al-2.98Be (at%) (A1) and Cu-22.60Al-3.26Be (at%) (A2) polycrystalline alloys were used in the present work. The chemical composition was determined by atomic absorption spectrophotometry. Prior to the heat treatment, the samples were kept during 5 min at 1073 K, in the β field, and water quenched at room temperature. In this way, a single β phase microstructure with a grain size of around 0.5 mm was obtained. The martensitic transformation temperatures (Ms) were determined from the slope change in temperature–time cooling rumps at 10 K/s, using a Cole-Parmer data acquisition module [7]. The measured temperatures were 252 K for the 3.26 at.% Be alloy, and 261 K for the 2.98 at.% Be alloy. Precipitation of dendritic γ_2 phase was generated by slow cooling at around 1.3 K/min from 1073 K to 808 K, followed by water quenching at room temperature. The temperature was monitored using a chromel–alumel thermocouple. The volume fraction of precipitates was approximately 14% in both alloys, estimated from optical micrographs. A detailed description is given in [18]. Samples around 2 mm length were cut using an Isomet Low Speed Saw with a diamond disc, from cylinders of 5 mm diameter. The samples were smoothed with 240, 600 and 1000 grit emery paper and then polished with alumina powder (0.3 μm size).

The specimens were observed using a JEOL JSM-6460LV scanning electron microscopy (SEM). Energy dispersive X-ray spectroscopy (EDX) analysis under SEM was employed to estimate the composition of different phases in the samples, and to obtain compositional profiles along lines covering the precipitates and the matrix.

Instrumented indentation was conducted with a Hysitron Triboindenter under load control at room temperature (around 22 °C). A Berkovich diamond indenter with a nominal radius of 100–200 nm and a total included angle of 142.3° was used. In the single β phase samples, series of three tests separated by 3 μm from each other were performed. The series, six at least, were carried out on different grains. On each test, sequential indentations with increasing levels of maximum load of 400 μN (four cycles at 15 μN/s), 2000 μN (four cycles at 60 μN/s) and 4000 μN (four cycles at 120 μN/s) were performed. In the $(\beta + \gamma_2)$ samples, series of twelve tests separated by 4 μm from each other were performed on the precipitates and the matrix. The series were carried out on different zones of the samples. Each test consisted of two cycles at 1500 μN (100 μN/s). A load–displacement plot was obtained for each indent.

Conventional Vickers indentations were conducted using a Mitutoyo MVK-H11 under a load of 50 g.

3. Results and discussion

3.1. Characterization of the β samples

Fig. 1(a) shows representative Berkovich tip indentations load–displacement (P–h) curves for the pseudoelastic β-A1 specimen, a single cycle and repeated cycles up to increasing levels of maximum load (P_{max}) of 400, 2000 and 4000 μN. No unloading–reloading path was included for the sake of clarity. The single cycle corresponds to the envelopment of the successive cycles. It can be seen that the load–displacement path in each cycle depends on the loading history, and the material "remembers" the maximum point of the previous cycle, at which unloading began, returning to this point upon the subsequent loading. Similar behavior was presented by β CuAlBe polycrystals subjected to compression tests [5].

In Fig. 1(b), four intermediate unloading–reloading curves for two P_{max}, 400 μN and 2000 μN, are included. The unloading–reloading paths form a closed hysteresis loop, which is highly repetitive. These distinct loops in shape-memory alloys are associated with some degree of pseudoelasticity because of a forward and reverse phase transformation [9,12,14]. It can be mentioned that broader loops have been observed with spherical indenter in NiTi alloys [12]. In the present alloy, the reversible phase transformation is a martensitic one, β ↔ 18R.

When pseudoelastic alloys like CuAlBe alloy are subjected to macroscopic compressive tests, three deformation stages can be identified. The typical pseudoelastic (PE) stress–strain cycles show a first linear part corresponding to the elastic regime of the β phase. A linearity deviation is associated with the β to martensite transformation start. A subsequent nearly constant stress–strain slope corresponds to the progress of the martensitic transformation, followed by plastic deformation. For a polycrystalline CuAlBe alloy with similar composition and at room temperature, the martensitic transformation starts at around 250 MPa, while macroscopic plasticity starts at a higher stress level, around 600 MPa [5]. On removing the load, a hysteresis loop is formed, and an almost complete strain recovery is obtained for PE strains up to around 3% [5]. Therefore, the indenter penetration effect upon increasing load could be associated with elastic, pseudoelastic, and plastic deformation. The important indentation depth recovery during unloading observed in Fig. 1 suggests that only a small portion is accommodated plastically, and most of the indenter displacement

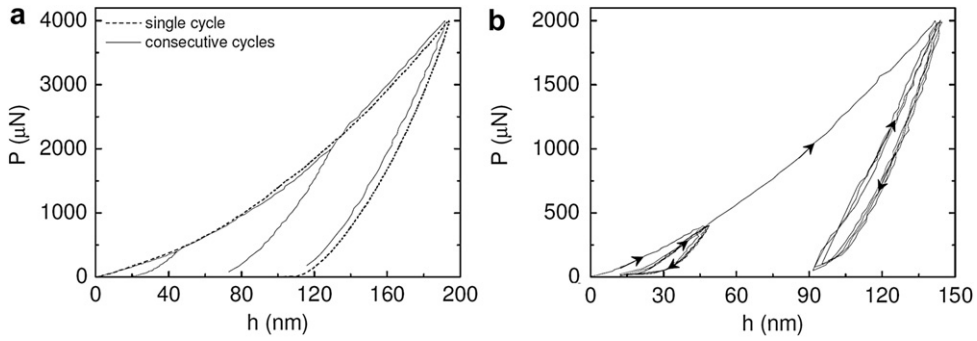

Fig. 1. P–h curves for the pseudoelastic β-A1 specimen: (a) A single cycle and consecutive cycles up to increasing levels of maximum load; (b) intermediate unloading–reloading curves for two P_{max}, 400 μN and 2000 μN.

corresponds to elastic and pseudoelastic deformation. The indentation depth recovery can be characterized by the recovered depth (h_{rec}), which is defined from indentation P–h curves as:

$$h_{rec} = h_{max} - h_f \quad (1)$$

where h_{max} is the indentation depth at P_{max}, and h_f is the final depth of the contact impression after unloading [21]. The measured recovered depth increases as P_{max} increases, as can be seen in Fig. 2. The considered depth components are indicated in the inset. The depth recovery ratio (η_h), defined as [10]:

$$\eta_h = h_{rec}/h_{max} \quad (2)$$

gives values of 0.41 ± 0.06 for A1, and 0.49 ± 0.07 for A2. These recovery ratios are similar to the values reported for a pseudoelastic NiTi alloy subjected to Berkovich indentations [10], which are also in the range of 0.4–0.5. No significant differences were appreciated for η_h obtained at various loads, as is expected for Berkovich indentations [10]. The obtained values of η_h in a pure elastic–plastic material like Cu are around 0.08 [10], remarkably lower than that obtained in pseudoelastic materials.

An average contact pressure (ACP) can be calculated dividing the applied load, P, by the contact area, a_c:

$$ACP = P/a_c \quad (3)$$

This parameter can be considered as a mean contact applied stress [9,14]. Following the Oliver and Pharr method [21], and using the tip-shape calibration made on fused quartz, the area function relating the projected contact area (a_c) to the contact depth (h_c) in the depth range of 33–177 nm was obtained as:

$$a_c = 24.5 \cdot h_c^2 + 10584 \cdot h_c^{1/2} + 10^{-6} \cdot h_c^{1/4} \quad (4)$$

with the contact depth given by:

$$h_c = h_{max} - h_s = h_{max} - 0.75 \cdot P_{max}/S \quad (5)$$

where h_s is the displacement of the surface at the perimeter of the contact, and S is the unloading contact stiffness, which corresponds to the slope of the initial portion of the unloading curve. It must be considered that equation (5) has been proposed for elastic–plastic materials, with S obtained in the elastic regime. In our case, unloading corresponds to elastic plus pseudoelastic recovery, and equation (5) is an approximation. h_s was obtained from indentation curves on both alloys at the different maximum loads using the equation (5). The calculated values are shown in Fig. 3, and an empirical relation between h_s and h_{max} was estimated obtaining:

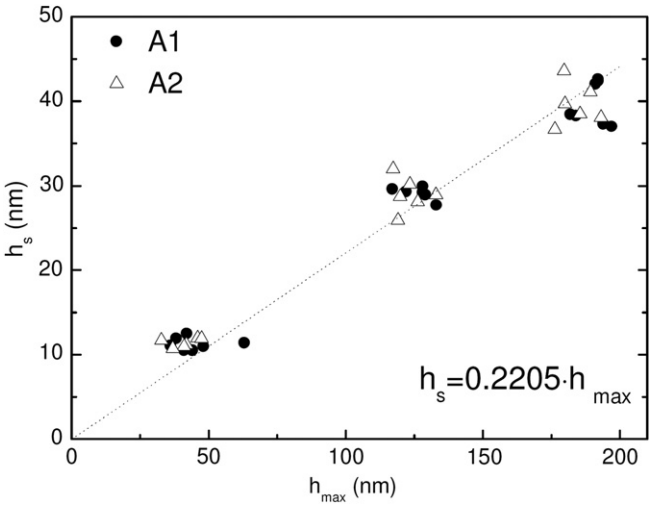

Fig. 3. Variation of h_s with h_{max} in β-A1 and β-A2 specimens.

$$h_s = 0.2205 \cdot h_{max} \quad (6)$$

with an R-squared value of 0.9403.

Using the equations (3)–(6), the ACP as a function of the penetration depth was obtained. Fig. 4 shows the ACP *versus* h obtained from representative indentations made on different zones of samples of both alloys at P_{max} = 400 μN. No marked differences were observed between the curves obtained on distinct zones or grains. It is known that the stress–strain behavior in uniaxial tests is strongly dependant on the β phase crystal orientation. On the other hand, it seems that some average behavior is obtained under Berkovich microindentation, because of the complex multiaxial stress state induced. An almost linear ACP increase is observed up to around 3 GPa and 15 nm of h, followed by a slope change, and a new almost linear regime. An important indentation depth recovery is observed on unloading. The ACP–h curves remind stress–strain pseudoelastic curves obtained under tensile as well compressive stress when pseudoelastic and/or plastic deformation

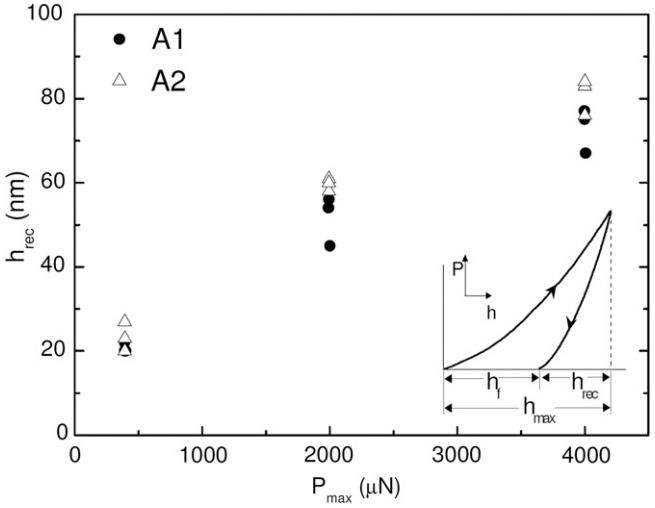

Fig. 2. Recovered depth upon unloading obtained for different maximum loads in β-A1 and β-A2 specimens.

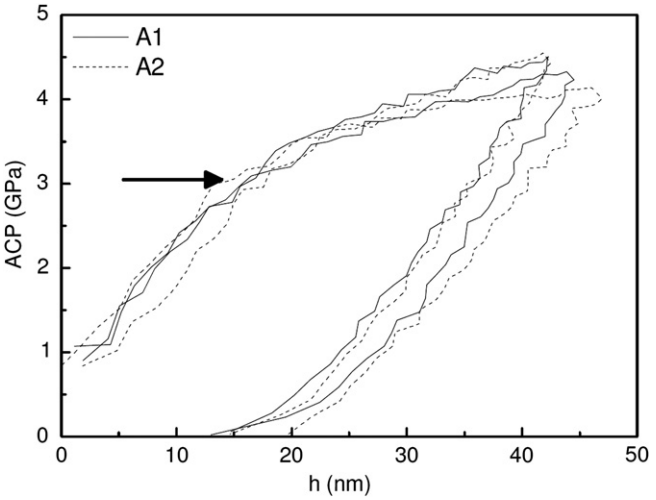

Fig. 4. ACP as a function of h for the pseudoelastic β-A1 and β-A2 specimens.

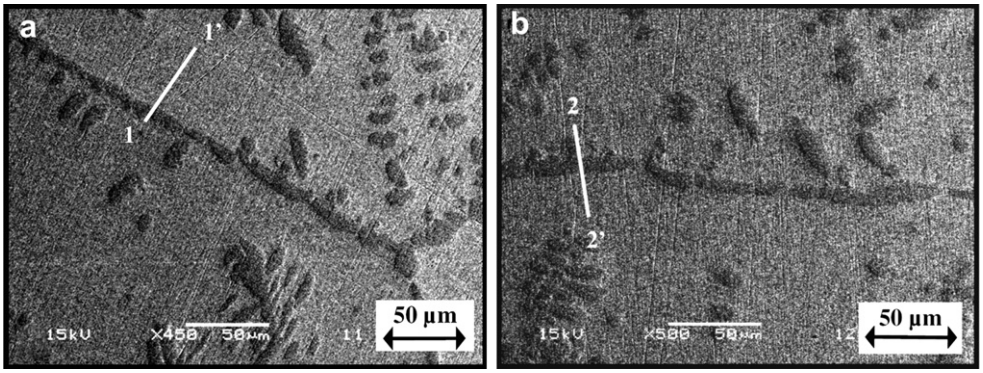

Fig. 5. Micrograph of ($\beta + \gamma_2$) samples corresponding to alloy A1 (a) and A2 (b) (backscattered electrons-SEM).

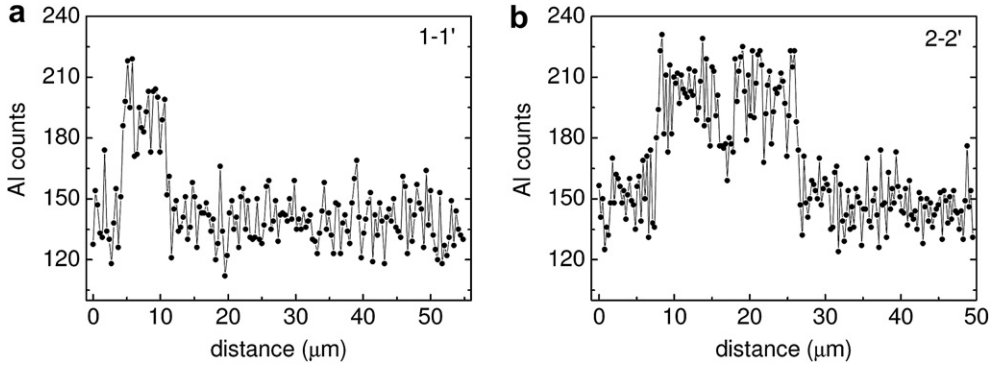

Fig. 6. Aluminum compositional profile along the lines 1–1′ (a) and 2–2′ (b) shown in Fig. 5.

is retained on unloading [5], although the stresses are not comparable because of the different stress states generated by the two types of tests [9,12]. The first linear ACP increase could be related to the elastic regime, and the subsequent stage to pseudoelastic plus plastic deformation. Similar ACP curves have been reported for Cu–Al–Ni and NiTi shape-memory alloys [12,14].

3.2. Indentations on samples with ($\beta + \gamma_2$) microstructure

The γ_2 precipitates were difficult to distinguish on polished samples using the detector of secondary electrons in SEM. However, they could be observed by backscattered electrons as darker areas, Fig. 5. The precipitates exhibit dendritic morphology and grain boundaries appear decorated by them in both alloys. It has been reported that grain boundaries are not preferential nucleation sites of γ_2 phase, but the precipitates nucleated there grow afterward along them [22].

Compositional profiles of aluminum along lines between the precipitates and the matrix in both alloys are given in Fig. 6. The EDX analysis results of the two phases in samples corresponding to both alloys and microstructures are given in Table 1. The errors were estimated as the standard deviation of the at least three measurements.

Table 1
EDX analysis of different phases of samples corresponding to both alloys. The balance is the Cu content.

Alloy	Microstructure	Aluminum content (%p)	
		β	γ_2
A1	β (β + γ_2)	13.6 ± 0.1	–
		12.9 ± 0.4	17.6 ± 0.3
A2	β (β + γ_2)	14.5 ± 0.1	–
		12.0 ± 0.2	16.7 ± 0.2

The results corroborate that the precipitates correspond to γ_2 phase, which is rich in aluminum and has a Cu_9Al_4 structure, as has been reported previously in alloys with a similar composition [23]. The matrix in the samples with a ($\beta + \gamma_2$) microstructure has aluminum contents slightly lower than those of the single phase samples due to precipitation. Almost no differences were found between the compositions estimated by EDX for both alloys. It can be observed in Fig. 6 that there is no detected significant aluminum compositional gradient in the β phase that surrounds the precipitates.

Series of indentations in direction perpendicular to the precipitates, along lines like that indicated in Fig. 5, were conducted in both alloys. Fig. 7 shows representative indentation P–h curves for the ($\beta + \gamma_2$)-A2 specimen. Curves A and B were obtained on the precipitates, and curves C and D were obtained on the matrix at a distance of 4 and 24 µm from the precipitate, respectively. The indentation response of the two phases is remarkably different. For a P_{max} of 1500 µN, the maximum displacement obtained in the precipitates is around 60 nm, while the maximum displacement reached in the matrix is almost the double (Fig. 7(a)). That large difference in the depth attained a maximum load reveals the difference in hardness between both phases, indicating that γ_2 is harder than β phase.

Fig. 7(b) shows unloading–reloading curves for both phases. While in the β phase a hysteresis loop is obtained, in the precipitates a complete coincidence between the unload and reload path is observed. As non-transforming phase, indentation on γ_2 produces elastic plus plastic deformation. Elastic recovery takes place during unloading which is reversed under reloading, leading to near

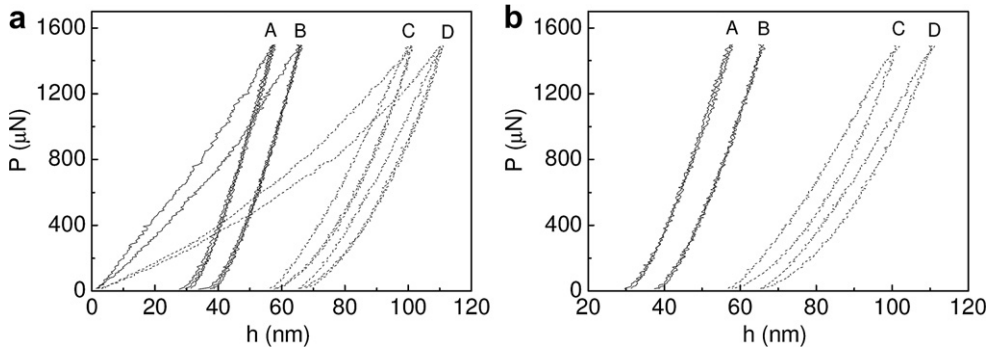

Fig. 7. Representative P–h curves for the ($\beta + \gamma_2$)-A2 specimen, performed on the precipitates (A and B) and on the β matrix (C and D): (a) first and second cycles, and (b) unloading and reloading curves.

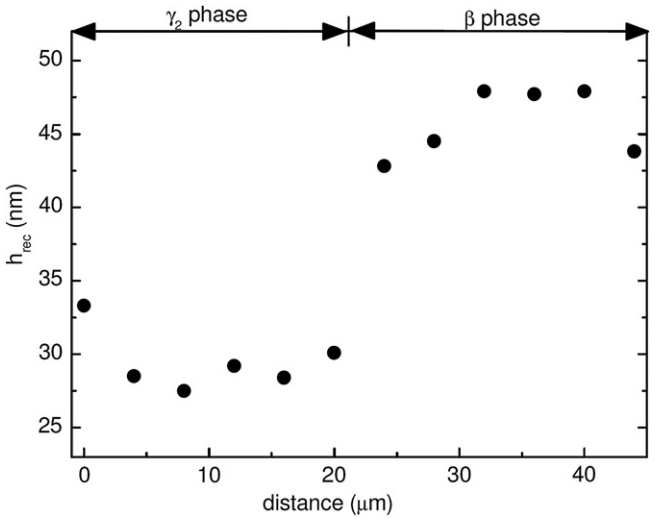

Fig. 8. Recovered depth upon unloading obtained for the series of indentations conducted on ($\beta + \gamma_2$)-A2 at $P_{max} = 1500$ μN.

perfect reversibility. This is the typical behavior of elastic–plastic materials obtained with a Berkovich indenter [16].

The recovered depth calculated using the equation (1) for the series of indentations conducted on A2 is presented in Fig. 8. The first points between 0 and 20 μm correspond to the precipitate and the other values correspond to the β matrix. Values of h_{rec} in the range of 45–50 nm are obtained in the matrix, which are similar to those extrapolated for P_{max} of 1500 μN in the β single phase microstructure in Fig. 2. The recovery capacity exhibited by γ_2 phase is lower, with h_{rec} around 30 nm. This difference between both phases is associated with the pseudoelastic behavior of the β phase.

The variation of ACP with the displacement was also estimated from the series of indentations conducted on A2, and representative ACP-h curves are presented in Fig. 9(a). For the precipitates ACP computation it was verified that the h_s–h_{max} relationship can be described within the experimental uncertainty by equation (6). Comparing the ACP–h curves for both phases, it can be noted that γ_2 phase exhibits higher ACP values, denoting its higher hardness. The transition ACP value between the two almost linear ACP–h stages was evaluated for each indentation (ACP_s), and it is shown in Fig. 9(b) for the series of indentations conducted on A2.

The ACPs is 7.7 ± 0.8 GPa in γ_2, and 3.3 ± 0.4 GPa in β phase. These values were calculated averaging those obtained on different zones or grains. As has been mentioned, the precipitates are an elastic–plastic material, so, no pseudoelastic deformation occurs, and pure elastic recovery takes place during unloading. A careful analysis of the ACP–h curves reveals that the unloading slope is similar to that of the first loading linear part in the γ_2 phase, suggesting that the first linear stage can be related to the elastic regime. On the other hand, the unloading slope does not coincide with the first loading slope in the β phase. This behavior could be explained because not only elastic but also pseudoelastic deformation is recovered during unloading in the transforming material. In this scheme, and besides more experimental tests are necessary, results suggest that 8 GPa and 3 GPa can be considered an elastic limit for γ_2 and β phase respectively under Berkovich indenter stress state.

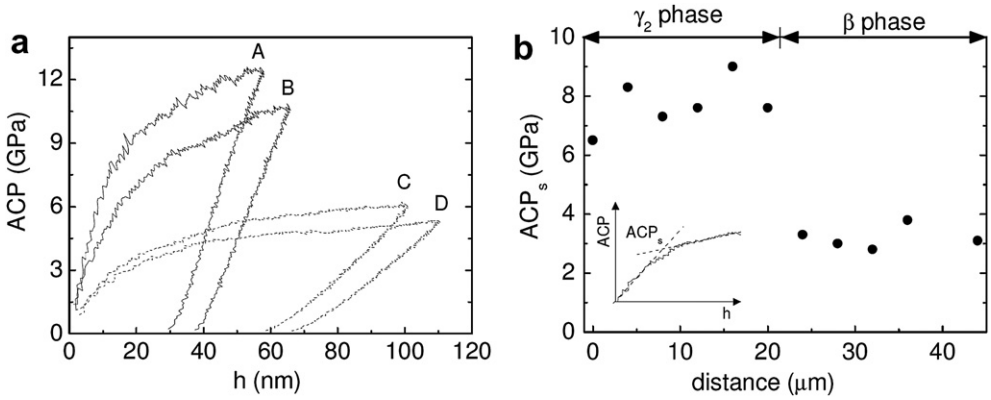

Fig. 9. (a) Variation of ACP with h during the first cycles obtained from data presented in Fig. 7. (b) ACP_s values for γ_2 and β phase.

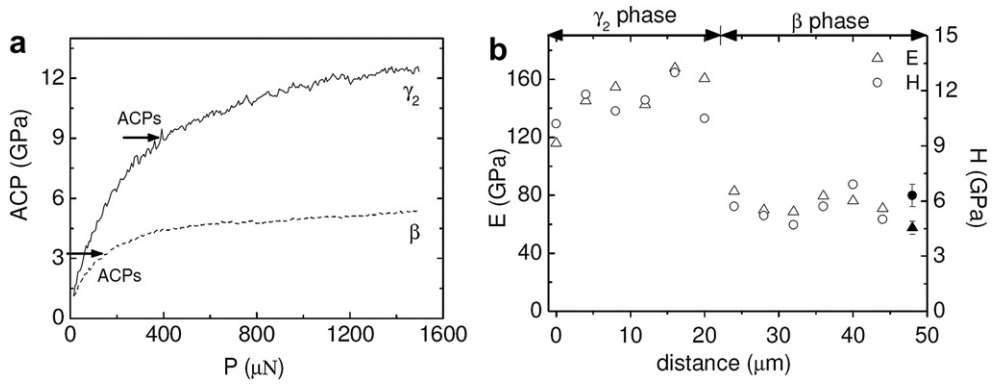

Fig. 10. (a) Variation of ACP with P obtained from loading curves presented in Fig. 9(a); (b) E and H obtained for the series of indentations conducted on $(\beta + \gamma_2)$-A2. Filled symbols correspond to the β single phase alloy.

It is important to note that the ACP, defined by equation (3), is a measure of the hardness H, normally defined as [21]:

$$H = P_{\max}/a_c \tag{7}$$

From Fig. 10(a), it can be seen that ACP increases as P increases. However, a slow variation is measured once the ACP_s is exceeded, what is clearly seen for the β phase. The H values for both phases obtained in β and $(\beta + \gamma_2)$ samples for $P_{\max} = 2000$ μN are shown in Fig. 10(b). The values of H and E obtained in β single phase alloys, and presented in Fig. 10(b), can be considered as an average of those measured in different grains. The Vickers hardness for $P_{\max} = 50$ g $(5{\cdot}10^5$ μN) of each phase was also determined in a sample with a volume fraction of γ_2 phase around 18%. The obtained hardness values were HV = (231 ± 6) for the matrix and HV = (477 ± 17) for the precipitates. It is interesting to note that the hardness of the precipitates is almost twice that of the matrix determined with both methods.

The elastic modulus (E) of both phases was estimated from load–displacement curves using the Oliver and Pharr method [21]. Following this method, the reduced modulus (E_r) was obtained by [21]:

$$E_r = S\sqrt{\pi}/2\sqrt{a_c} \tag{8}$$

S was obtained from the unloading curves, and a_c was estimated using equation (4). E was then calculated through the following relation [21]:

$$1/E_r = \left(1 - \nu^2\right)/E + \left(1 - \nu_i^2\right)/E_i \tag{9}$$

where ν is the Poisson's ratio of the material tested and E_i and ν_i are the modulus and Poisson's ratio of diamond. The Poisson's ratio used for the material was 0.3 [24,25] and the constants used for the diamond were: $E_i = 1141$ GPa and $\nu_i = 0.07$ [21].

The values of E for both phases, estimated for indentation curves with $P_{\max} = 2000$ μN, are shown in Fig. 10(b). An average value of (74 ± 6) GPa for the β phase, and of (148 ± 18) GPa for the γ_2 phase was obtained. No significant difference was found for E obtained in both alloys and for indentation curves at other $P_{\max}$ (400 and 4000 μN). Even when the indentations at various $P_{\max}$ were performed at different loading speeds, it does not significantly influence on the determination of E, as has been reported previously in other alloys [26]. It is important to note that E does not strictly correspond to β phase, because it is expected that some fraction of martensite phase is present in the samples when the unloading begins. Similar values have been reported in other β Cu–Al–Be polycrystalline alloys in the range of 53–75 GPa [27–29], determined by tensile and ultrasound tests.

4. Conclusions

The behavior of β and γ_2 phases in Cu–Al–Be alloys under instrumented indentation using a Berkovich tip was studied in load ranges between 400 μN and 4000 μN.

The pseudoelastic effect in the β phase is evidenced by closed hysteresis loops between the unloading–reloading paths in the P–h curves. The high depth recovery ratios are similar to the values reported for pseudoelastic NiTi alloys.

From series of indentations conducted in the $(\beta + \gamma_2)$ specimens, it was found that the indentation response of the two phases is remarkably different:

a) While in the β phase a hysteresis loop is obtained, in the precipitates a complete coincidence between the unload and reload path is observed, which is associated with the elastic–plastic behavior of the γ_2 phase.
b) The recovery capacity exhibited by the β phase is higher than that by the γ_2 phase, which is related to the transforming character of β.
c) The larger depth attained in the matrix reveals the difference in hardness between both phases, indicating that γ_2 is harder than β phase.
d) An average contact pressure *versus* the penetration depth curve was estimated for each indentation curve. Results suggest that 8 GPa and 3 GPa can be considered an elastic limit for γ_2 and β phase respectively under Berkovich indenter stress state.
e) The elastic modulus and hardness of both phases were estimated from load–displacement curves using the Oliver and Pharr method, obtaining higher values of both parameters for γ_2 phase. However, it is important to note that E does not strictly correspond to β phase, because it is expected that some fraction of martensite phase is present in the samples when the unloading begins.

Acknowledgments

This work was supported by ANPCYT, CONICET, Universidad Nacional de Mar del Plata and SECAT-UNCentro.

References

[1] Hautcoeur A, Eberhardt A, Patoor E, Berveiller M. Thermomechanical behaviour of monocrystalline CuAlBe shape memory alloys and determination of the metastable phase diagram. J Phys IV 1995;C2-5:459–64.

[2] Cingolani E, Stalmans R, Van Humbeeck J, Ahlers M. Influence of thermal treatments on the long range order and the two way shape memory effect induced by stabilization in Cu–Al–Be single crystals. Mater Sci Eng A 1999; 268:109–15.
[3] Kustov S, Pons J, Cesari E, Morin M, Van Humbeeck J. Athermal stabilization of Cu-Al-Be β'_1 martensite due to plastic deformation and heat treatment. Mater Sci Eng A 2004;373:328–38.
[4] Kaouache B, Berveiller S, Inal K, Eberhardt A, Patoor E. Stress analysis of martensitic transformation in Cu–Al–Be polycrystalline and single-crystalline shape memory alloy. Mater Sci Eng A 2004;378:232–7.
[5] Montecinos S, Cuniberti A. Thermomechanical behavior of a CuAlBe shape memory alloy. J Alloys Compd 2008;457:332–6.
[6] Montecinos S, Cuniberti A, Sepúlveda A. Grain size and pseudoelastic behaviour of a Cu–Al–Be alloy. Mater Charact 2008;59:117–23.
[7] Montecinos S, Cuniberti A, Romero R. Effect of grain size of the stress-temperature relationship in a β CuAlBe shape memory alloy. Intermetallics 2011;19:35–8.
[8] Montecinos S, Cuniberti A. Aplicación de aleaciones con memoria de forma CuAlBe en amortiguamiento pasivo de estructuras civiles. Revista SAM 2009; 6(3):20–9.
[9] Frick CP, Lang TW, Spark K, Gall K. Stress-induced martensitic transformations and shape memory at nanometer scales. Acta Mater 2006;54:2223–34.
[10] Ni W, Cheng Y-T, Grummon DS. Microscopic shape memory and superelastic effects under complex loading conditions. Surf Coat Technol 2004;177–178: 512–7.
[11] Liu R, Li DY, Xie YS, Llewellyn R, Hawthorne HM. Indentation behavior of pseudoelastic TiNi alloy. Scr Mater 1999;41(7):691–6.
[12] Arciniegas M, Gaillard Y, Peña J, Manero JM, Gil FJ. Thermoelastic phase transformation in TiNi alloys under cyclic instrumented indentation. Intermetallics 2009;17:784–91.
[13] Amini A, Yan W, Sun Q. Depth dependency of indentation hardness during solid-state phase transition of shape memory alloys. Appl Phys Lett 2011;99: 021901.
[14] Zhang HS, Komvopoulos K. Nanoscale pseudoelasticity of single-crystal Cu–Al–Ni shape-memory alloy induced by cyclic nanoindentation. J Mater Sci 2006;41:5021–4.
[15] Crone WC, Brock H, Creuziger A. Nanoindentation and microindentation of CuAlNi shape memory alloy. Exp Mech 2007;47:133–42.
[16] Oliver WC, Pharr GM. Measurement of hardness and elastic modulus by instrumented indentation: advances in understanding and refinements to methodology. J Mater Res 2004;19(1):3–20.
[17] Liu XJ, Ohnuma I, Kainuma R, Ishida K. Phase equilibria in the Cu-rich portion of the Cu–Al binary system. J Alloys Compd 1998;264:201–8.
[18] Montecinos S, Cuniberti A, Castro ML, Boeri R. Phase transformations during continuous cooling of polycrystalline β-CuAlBe alloys. J Alloys Compd 2009; 467:278–83.
[19] Swann PR, Warlimont H. The electron-metallography and crystallography of copper–aluminum martensites. Acta Metall 1963;11:511–27.
[20] Belkahla S, Flores Zuñiga H, Guenin G. Elaboration and characterization of new low temperature shape memory Cu–Al–Be alloys. Mater Sci Eng A 1993;169:119–24.
[21] Oliver WC, Pharr GM. An improved technique for determining hardness and elastic modulus using load and displacement sensing indentation experiments. J Mater Res 1992;7(6):1564–83.
[22] Cuniberti A, Montecinos S, Lovey FC. Effect of γ_2 phase precipitates on the martensitic transformation of a β-CuAlBe shape memory alloy. Intermetallics 2009;17:435–40.
[23] Montecinos S, Simison SN. Influence of the microstructure on the corrosion behaviour of a shape memory Cu–Al–Be alloy in a marine environment. Appl Surf Sci 2011;257:2737–44.
[24] Bouvet C, Calloch S, Lexcellent C. Mechanical behavior of a Cu–Al–Be shape memory alloy under multiaxial proportional and nonproportional loadings. Trans ASME 2002;124:112–24.
[25] Entemeyeer D, Patoor E, Eberhardt A, Berveiller M. Strain rate sensitivity in superelasticity. Int J Plasticity 2000;16:1269–88.
[26] Cai J, Li F, Liu T, Chen B. Investigation of mechanical behavior of quenched Ti-6Al-4V alloy by microindentation. Mater Charact 2011;62:287–93.
[27] Casciati F, Faravelli L. Experimental characterization of a Cu-based shape memory alloy toward its exploitation in passive control devices. J Phys IV 2004;115:299–306.
[28] de Albuquerque VHC, Melo TA de A, de Oliveira DF, Gomes RM, Tavares JMRS. Evaluation of grain refiners influence on the mechanical properties in a CuAlBe shape memory alloy by ultrasonic and mechanical tensile testing. Mater Des 2010;31:3275–81.
[29] Gédouin P-A, Chirani SA, Calloch S. Phase proportioning in CuAlBe shape memory alloys during thermomechanical loadings using electric resistance variation. Int J Plasticity 2010;26:258–72.